SOH Modelling of Li-Ion Coin Cells Subjected to Varying C-Rates, Depths of Charge, Operating Temperatures and Custom Charge Profiles

Pradeep Lall
NSF-CAVE3, Electronic Research Center,
Department of Mechanical Engineering,
Auburn University, Auburn, AL. 36849.
Email – lall@auburn.edu

Ved Soni
NSF-CAVE3, Electronic Research Center,
Department of Mechanical Engineering,
Auburn University, Auburn, AL. 36849.
Email – vzs0040@auburn.edu

Guneet Sethi
Amazon Lab 126,
Sunnyvale, CA.

Kok Yiang
Amazon Lab 126,
Sunnyvale, CA.

***Abstract* – Portable consumer electronics devices continue to be one of electronics high-demand items, with rising interest in such products recently. Li-Ion batteries are the most popular power source choice of these products owing to a combination of high specific energy and specific power. In consumer electronics products, these batteries are generally employed in their coin form factor in biomedical devices, sensors, wireless earbuds, etc. These developments have boosted the research effort on Li-Ion power sources, and a major part of this effort is the prognostics of Li-Ion battery state of health (SOH) and predicting its remaining useful life. In addition to the common operation and environmental parameters such as the C-rate, the surrounding temperature and the depth of charge, additional parameters such as custom charge profiles employed by products need to be considered while modelling battery SOH degradation. This study focuses on the development of a SOH estimation model for two types of Li-ion coin cells subjected to accelerated life testing along with varying C-rates, operating temperature and depths of charge. Moreover, a custom charge profile wherein the charging current supplied to the battery was modified throughout its life cycle depending upon its instantaneous capacity was experimented to see its effect on the SOH degradation rate. Finally, regression models, focusing on the relation between SOH degradation and battery use parameters was developed.**

Keywords - capacity degradation, state of health, consumer electronics, SOH modelling, RUL modelling, li-ion battery, coin cell.

I. INTRODUCTION

The lithium-ion battery is the most popular choice of electrical energy storage technology in current portable consumer electronics devices owing to its great combination of high specific energy and high specific power [1][2]. Apart from consumer electronics products, applications such as smartcards, radio frequency-based identification tags (RFID), and biomedical sensors [3][4][5] have adopted this battery technology in either its coin or pouch form factor due to dimensional constraints. Thus, this has given an impetus to the research and development in ultra-thin pouch cells from the new perspectives of compactness and flexibility in addition to the usual areas of focus such as higher capacity, faster charging currents, greater operating temperature range and low degradation rate. Within the past two decades, there has been an abundance of experimental research published on lithium ion battery degradation wherein power sources are subjected to accelerated life cycling in combination with several operating conditions such as extreme currents, temperatures, variations in the charge/discharge depths, etc. [6][7][8][9].

Some of the main purposes of lithium-ion battery degradation research are: the identification of electrochemical failure modes of batteries so as to optimize the battery design while enhancing its safety, and development of methods to estimate the battery capacity degradation to determine its end-of-life (EOL), which is also known as battery health prognostics. The battery failure mode research has reached its maturity whereas the battery health prognostics is currently gaining momentum owing to a plethora of artificial intelligence-based methods being used to tackle this complex problem. Battery health prognostics generally involves building a mathematical model for estimating the current 'state of health' and thereby predicting the remaining useful life (RUL) of a battery as a function of the number of charge-discharge cycles and the operating conditions it has been subjected to. State of health is defined as the ratio of the battery's current capacity to its nominal capacity converted to a percentage form [10] as seen in (1). A battery is considered to have reached its end-of-life when its capacity has degraded to 80% of its nominal value [10].

$$\text{SoH} = \frac{\text{Battery Capacity}}{\text{Rated Capacity}} * 100 \quad (1)$$

Lithium-ion battery degradation models are of three main kinds: electrochemical models, equivalent circuit models and data-driven models [10]. The electrochemical models model the battery using physics-based equations which represent the battery behavior and its underlying degradation mechanisms. Owing to their complexity, they are mainly used by battery designers and are unavailing for the end-users of commercial batteries. The second kind of models are equivalent circuit models which represent the battery as an electrical circuit using simple electrical elements such as resistors, capacitors, etc. Data of battery impedance is determined experimentally using techniques such as electrochemical impedance spectroscopy (EIS); the cost of

performing EIS is the major hindrance to developing these models.

The last type of models are data driven models which rely on physical quantities such as terminal voltage, battery current, battery capacity, cell impedance, etc. recorded over the entire test duration to estimate the capacity degradation. Data driven methods can further be classified into differential analysis, empirical models and machine learning (ML) based models. Differential analysis methods such as incremental capacity/differential voltage (IC/DV) curves are not applicable widely owing to operating condition limitations. Semi-empirical and empirical models rely on fitting the raw data using nonlinear regression models along with several state estimation techniques such as Kalman filters, particle filters, etc. Machine learning methods are being rapidly explored for battery health prognostics as they offer higher accuracy in comparison to the methods discussed earlier. However, apart from being computationally intensive, these models have low interpretability, i.e. they do not clearly define the dependency of the output on several inputs used for model development. The interpretability factor is significant from a research point of view as it may point towards the underlying physics of battery capacity degradation.

For the current study, a semi-empirical technique using nonlinear regression has been used for model building. Literature on these types of models exists since the last decade on various lithium-ion battery chemistries but is not too well developed. Several experimental studies have been conducted to investigate the effect of different use conditions on calendar and cycle ageing which have later been captured via non-linear regression models.

Hoog [11] developed a cycling capacity fade model for Li-ion batteries with NMC cathode having a rated capacity of 20 Ah based on the number of charge-discharge cycles, the depth of discharge and the charging range. Charging range is basically the initial capacity (%) of the battery before charging and the final capacity (%) after charging. The relative capacity degradation was the model output and the expression is given by (2):

$$\mathrm{RCD}(x,y) = \sum_{i=0,j=0}^{n,m} a_i x^i + b_j y^j \quad (2)$$

Where '*x*' is the number of charge-discharge cycles and '*y*' is the depth of discharge. The variation of *RCD* with charging range was represented in a graphical format rather than including it as a model variable. Finally, tests with varying operating temperatures were also conducted and the dependence of the degradation was explained using the Arrhenius relation.

Stroe [12] investigated the effect of accelerated life testing with variation in operating temperature on LiFePO4/C Li-ion batteries. They built a nonlinear regression model considering the effects of the cycle number and temperature on the percent capacity degradation (3):

$$Q_{Deg}(\%) = 6.87*10^{-5} e^{0.027T} (NC)^{0.5} \quad (3)$$

Sarasketa-Zabala [13] experimented with 2.3 Ah LiFePO4 Li-Ion batteries and established a cycling ageing model to explain battery degradation for different ranges of depths of discharge of the battery. The model equations are as follows (4) (5):

(i) For 10% < DOD < 50% (4)

$$Q_{Loss}(\%) = \left(\gamma_1 DOD^2 + \gamma_2 DOD + \gamma_3\right) k(Ah)^{0.87}$$

(ii) For DOD<10% and DOD>50% (5)

$$Q_{Loss}(\%) = (\alpha_3 e^{\beta_3 DOD} + \alpha_4 e^{\beta_4 DOD}) k(Ah)^{0.65}$$

Where Ah is the charge throughput in ampere-hours through the battery. The major shortcoming of these models is the lack of extensiveness in incorporating different use conditions such as the C-rate, temperature, charge/discharge depth, etc. in one single model.

The current study is similar to those performed by Lall [14]. This work focuses on development of a universal regression model which can capture the effect of charge-discharge current rate, operating temperature, and charge and discharge depth on the capacity degradation of lithium-ion battery subjected to accelerated life testing. Experimental testing of batteries has been carried out using combinations of these use parameters and the gathered data is further processed before using it for creation of SOH estimation models.

II. Experimental Methodology

A. Test vehicle

Two commercially available coin cells with cell A having a capacity of 90 mAh and a dimensionally larger cell B having a capacity of 120 mAh were chosen as test vehicles for the present study. Both the cells had similar datasheet-specified cathode-anode chemistry (LiNiMnCoO2 (NMC) – graphite) as well as charge-discharge characteristics but differed only in their capacity and dimensions. TABLE I summarizes the electrochemical attributes of both the cells:

TABLE I. Physical Properties of Test Vehicles

Property	Cell A	Cell B
Nominal Capacity (mAh)	90	120
Nominal Voltage (V)	3.7	3.7
Operating Temperature (charging) (°C)	0 to 45	0 to 45
Operating Temperature (discharging) (°C)	-20 to 60	-20 to 60

TABLE II. Charge-Discharge Characteristics of Test Vehicles

Property	Cell A	Cell B
End of Charge Voltage (V)	4.2	4.2
Charge Current Range (mA)	45 (0.5C) to 180 (2C)	60 (0.5C) to 240 (2C)
End of Charge Current (mA)	1.7	2.4
End of Discharge Voltage (V)	3	3

A constant current-constant voltage (CCCV) charge profile has been used for battery charging and a constant current profile has been used for discharging. TABLE II enlists the manufacturer-specified charge-discharge profile characteristics for both the cells:

B. Experimental setup

An experimental testbed was designed and assembled for conducting the accelerated life testing of the battery samples subjected to various conditions. Fig. 1 details the schematic of the test setup and highlights its individual components.

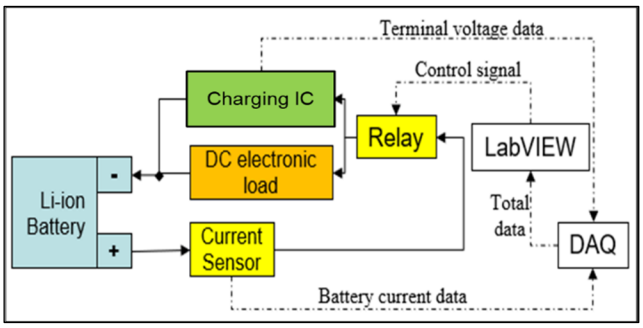

Fig. 1. Schematic Diagram of Test Setup

The coin cells held by a cell holder are connected alternately to the charging and discharging equipment via a SPDT relay board. A programmable charger IC with a switching topology has been used for charging the coin cells and a non-programmable DC electronic load has been used for the purpose of discharging. A data acquisition unit is used to measure the battery terminal voltage as well as the battery current via the current sensor. The battery voltage, current and elapsed time are recorded to the computer via LabVIEW which also uses the recorded values to automate the accelerated life cycling test for the required number of cycles. For high temperature testing of coin cells, they have been placed inside an environmental chamber while the test setup automates the test from an external ambient environment.

After the experimental testing of the samples, the raw data is then processed to compute the battery capacity and state of health which are then plotted against the cycle number and are also used for the regression model development. Following are the formulae used for computing the battery capacity (6) and SOH (7):

$$Q = \sum (I_{discharge} * t_{sampling}) \quad (6)$$

$$SOH = \frac{Q_{n^{th}\ cycle}}{Q_{rated}} \quad (7)$$

For SOH computation, the initial SOH values for all the samples tested are normalized to 100%; this facilitates the comparison of the rates of degradation due to different test conditions and ignores the pre-accumulated calendar aging effects.

C. Test Procedure and Matrices

Accelerated life testing has been conducted on battery samples to evaluate the effect of five different use parameters:

- Constant Charging C-Rate
- Constant Discharging C-Rate
- High Temperature Operation
- Depth of Charge
- Dynamic Charging C-Rate

As mentioned earlier, 80% state of health is the industry-accepted limit for failure of Li-ion batteries. Hence, most of the tests are run until the battery SOH drops below the 80% SOH failure limit. However, in some of the tests, it has been observed that the slope of the degradation curve is less steep and remains constant after about 100 cycles. Such tests have been terminated prior to the 80% SOH limit is attained, as the rate of degradation is the main component of interest for developing physical as well as application-based regression models using the gathered data.

The constant charging and discharging C-rate tests are the most basic ones performed wherein the accelerated life testing is conducted with a set charging and discharging C-rate throughout the test duration. For high temperature operation test case, as mentioned earlier, the cell is placed inside a environmental chamber set at a constant temperature. For depth of charge testing, one charge-discharge cycle comprises of the battery being charged up to a specified state of charge (%) and is then fully discharged to a 0% SOC. However, to measure the total capacity of the battery, three full charge-discharge cycles are performed after every 50 cycles of shallow depth of charge testing.

The idea behind the dynamic charging C-rate test is that, as the battery capacity degrades, the charging current will drop to a value which will be computed using the instantaneous capacity of the battery rather than its nominal capacity. For example, for cell A, the initial capacity is ~ 90 mAh, and thus, the 2C charging current would be 180 mA. As the cell capacity drops below 80 mAh due to continuous cycling, the dynamic charging C-rate protocol would adjust the instantaneous 2C charging current to 160 mA. Thus, as the instantaneous capacity of the battery degrades by 10 mAh, the charging C-rate would adjust accordingly. The 10 mAh step size is chosen because the charging IC supports minimum increments/decrements of 20 mA. Accordingly, dynamic charge C-rate tests are conducted for both the cells for 2C and 2.5C charge C-rates. TABLE III enlists the capacity and corresponding charge current used for both the cells for 2C and 2.5C dynamic charge C-rate tests:

TABLE III. BATTERY CHARGE CURRENTS FOR DYNAMIC CHARGE PROFILE

Cell A			
Capacity (mAh)	90	80	70
Charge Current (Dynamic 2C) (mA)	180	160	140
Charge Current (Dynamic 2.5C) (mA)	220	200	180
Cell B			
Capacity (mAh)	120	110	100
Charge Current (Dynamic 2C) (mA)	240	220	200

TABLE IV. TEST MATRIX FOR CELL A

Sr. No.	Charge C-Rate	Discharge C-Rate	Operating Temper-ature (°C)	Depth of Charge (%)	Dynami c Charge Profile	No. of repli-cates
1	2C	0.5C	25	100	N	2
2	1.5C	0.5C	25	100	N	2
3	1.5C	1C	25	100	N	1
4	1.75C	1C	25	100	N	2
5	1.5C	1C	25	75	N	2
6	1.5C	1C	25	50	N	2
7	1.5C	1C	40	100	N	1
8	2C	1C	25	100	Y	3
10	2.5C	1C	25	100	N	1
TOTAL						16

Multiple tests were conducted with different levels of various use parameters mentioned in this section earlier. Moreover, more than one samples were tested at some conditions to improve the fidelity of the data gathered and to ultimately enhance the model performance and reliability. TABLE IV and TABLE V enlist the test cases completed for cell A and cell B respectively.

TABLE V. TEST MATRIX FOR CELL B

Sr. No.	Charge C-Rate	Discharge C-Rate	Operating Temper-ature (°C)	Depth of Charge (%)	Dynami c Charge Profile	No. of repli-cates
1	2C	0.5C	25	100	N	3
2	2C	1C	25	100	N	1
3	1.5C	1C	25	100	N	2
4	1.75C	1C	25	100	N	2
5	2C	1C	40	100	N	2
6	1.5C	1C	25	100	Y	4
TOTAL						14

D. Use Parameter-Based Regression Model Development

As previously stated, the battery SOH was predicted using different input variables with a nonlinear semi-empirical regression model. Following were the use parameters to be accommodated into the regression model:

(i) Number of charge-discharge cycles
(ii) C-Rate and D-Rate
(iii) Operating Temperature
(iv) Depth of Charge
(v) Use of dynamic charging profile

The developed model had the following general form (8):

$$y = 100 - a x_1^{b_1} x_2^{b_2} \ldots x_n^{b_n} \tag{8}$$

Where a is the constant of proportionality and the b_i's are constants which denote the power law dependence of each input variable on the battery state of health. Since the maximum state of health of the battery sample can be 100%, the model was formulated to subtract the degradation estimated by the parameters from the maximum state of health. A general rule followed while defining input variables was to normalize all the variables to a similar input range so as to reduce the model error. Hence, instead of using the number of charge-discharge cycles as an input variable directly, its ratio with the maximum number of cycles was considered (9).

$$N = \frac{\text{Cycle Number}}{\text{Max Cycle Number}} \tag{9}$$

One commonly raised concern regarding the use of charge-discharge cycles as an input variable is that they do not account for the varying cycle depths and hence cumulative charge throughput is often recommended as an input variable instead of charge-discharge cycle number. However, since the depth of charge is considered as a separate variable in the regression model, the charge-discharge cycle number will be used as it is to reduce computational effort.

The charge and discharge C-rates are accommodated in a single variable C and its computation would be detailed further in the results section. Owing to the Arrhenius dependence of chemical reactions on the surrounding temperature, the temperature proportionality was considered as follows (10):

$$\text{SOH} \propto e^{b\left(\frac{1}{T}-\frac{1}{298}\right)} \tag{10}$$

Where e is the exponential number, b is a model constant and T is the operating temperature in Kelvin. Here too, the ratio of the given temperature condition to the 25°C (298 K) operating condition was considered for normalization. The effect of depth of charge was the most complicated to model as it isn't linearly proportional to the SOH, which is why its fractional value cannot be directly included as a variable in the model. After experimenting with several options, the integrated voltage was chosen to represent the cycle depth IV (11):

$$\text{IV} = \frac{\sum V_{\text{shallow}} t_{\text{shallow}}}{\sum V_{\text{deep}} t_{\text{deep}}} \tag{11}$$

The cycle depth is the ratio of cumulative sum of the product of voltage and time during the entire shallow cycle (charge and discharge) to the same cumulative sum for the deep cycle. In other words, it represents the average voltage and time at which the battery operates for a given depth of charge. The advantage of this variable over the direct depth of charge fraction is that IV can capture the battery degradation resulting from a high battery potential and the time spent at that potential. No special variable was used for the dynamic charge profile data, and the value of the charge current used during different stages of the accelerated life test was converted into C-rate values based on the battery's nominal capacity. Thus, the data entries for dynamic charge profile matched that of constant charge profile. Thus, the equation for the battery SOH model was as follows (12):

$$\text{SOH} = 100 - b_0 N^{b_1} C^{b_2} e^{b_3\left(\frac{1}{T}-\frac{1}{298}\right)} \text{IV}^{b_4} \tag{12}$$

The generated test data was used to determine the model coefficients. To test the robustness of the model, a 10-fold cross-validation test will be conducted. Individual models will be developed for both the cells by incorporating the generated test data.

III. EFFECT OF USE PARAMETERS ON SOH

The current section showcases the plots of the battery current and terminal voltage for both the test vehicles followed by their SOH degradation profiles under various

testing conditions. The results are also presented in a comparative manner which makes it easy to study the effect of individual test parameters. However, the current section only deals with the presentation of the results obtained whereas their explanation and justification are included in the next section.

A. Battery Current and Terminal Voltage Plots

Fig. 2 represents the plots of battery current and terminal voltage for one discharge-charge cycle against time for cell A for 1C D-rate and 1.5C C-rate. The discharge current is considered as negative and the charge current is considered as positive for this study. As can be seen from the annotations in Fig. 2, the CC discharge profile followed by a CCCV charge profile is conducted. Fig. 3 represents the same parameters plotted for cell B for 1C D-rate and 2C C-rate.

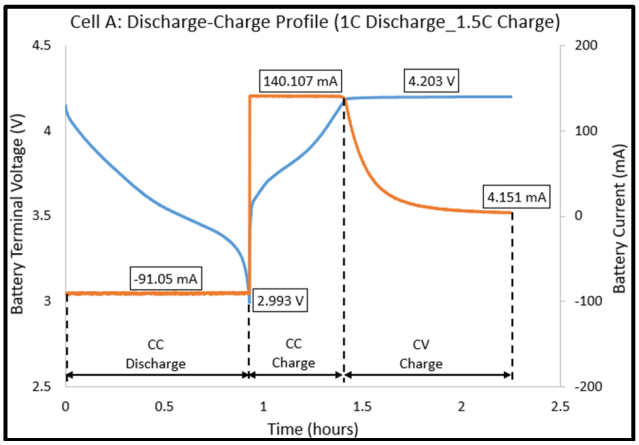

Fig. 2. Battery discharge-charge current and voltage profile for cell A

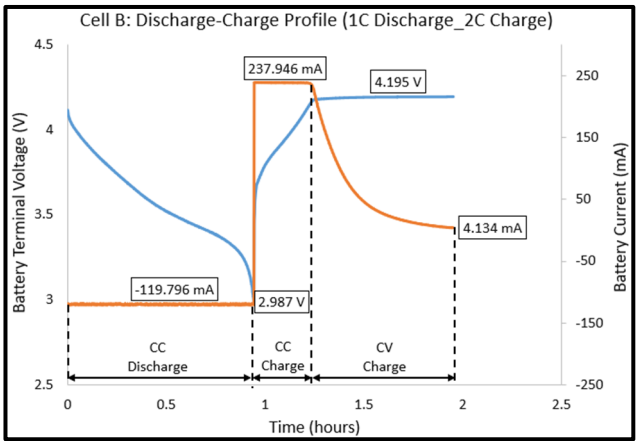

Fig. 3. Battery discharge-charge current and voltage profile for cell B

Finally, Fig. 4 and Fig. 5 depict the evolution of the battery current and battery terminal voltage curves respectively for deep cycling for cell A for 1C D-rate and 1.5C C-rate for the entire duration of the accelerated life cycling test. As the cycles progress, the current and voltage curves shift towards the left due to reduced discharge time, which is indicative of deteriorating battery state of health.

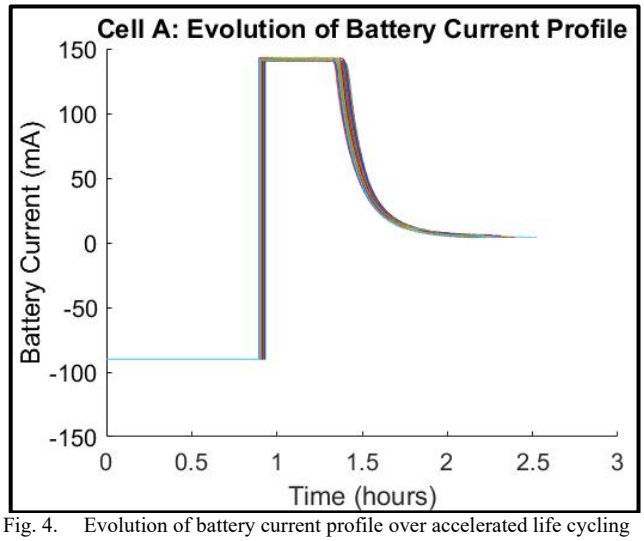

Fig. 4. Evolution of battery current profile over accelerated life cycling test for cell A

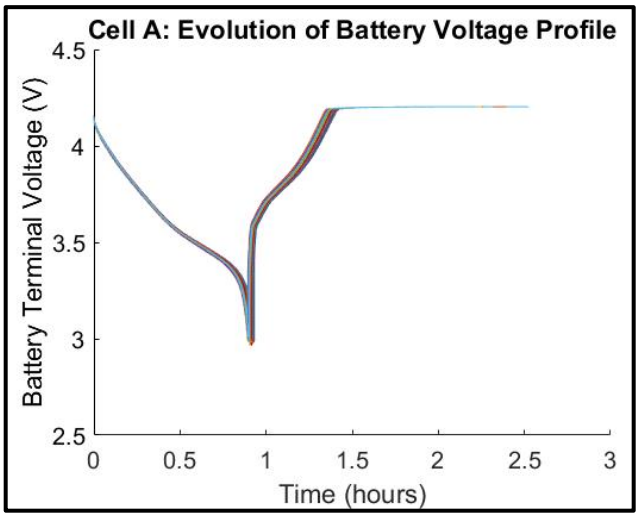

Fig. 5. Evolution of battery voltage profile over accelerated life cycling test for cell A

B. SOH Degradation: Effect of D-rate

Fig. 6 represents the battery state of health v/s charge-discharge cycle number curves for samples cycled deeply with 1.5C C-rate, but with different D-rates of 0.5C and 1C at 25°C.

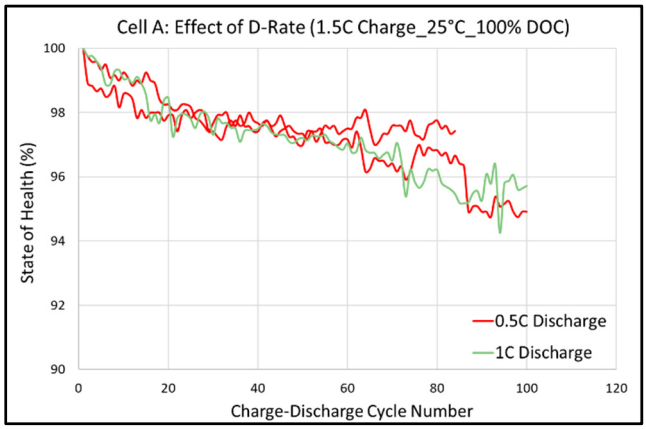

Fig. 6. Effect of discharge rate on the SOH degradation for cell A

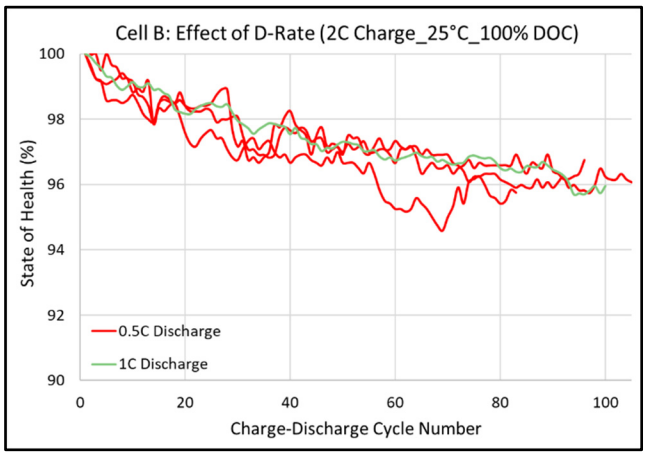

Fig. 7. Effect of discharge rate on the SOH degradation for cell B

As can be seen, the cases with differing D-rates follow the same degradation profile, which implies that changing the D-rate does not affect the SOH degradation of cell A significantly. Fig. 7 depicts similar plots for cell B cycled deeply with 2C C-rate at 25°C with D-rates of 0.5C and 1C. A similar trend can be seen in the degradation profiles of cell B as that of cell A. Thus, due to the insignificance of D-rate in affecting the battery state of health degradation, the D-rate has been eliminated as a predictor variable in the physical regression model development process.

C. SOH Degradation: Effect of C-rate

Fig. 8 depicts the degradation profile for cell A samples tested with differing C-rates ranging from 1.5C to 2.5C. As mentioned earlier, multiple samples have been tested at each condition for improving the fidelity of input data to the regression model. However, for easier comparison, Fig. 9 presents the same chart with averaged plots for each case of C-rate along with error bars indicating the standard deviation. Since all the samples were not tested till the same number of charge-discharge cycles, the averaged chart showcases results until only the 100th cycle.

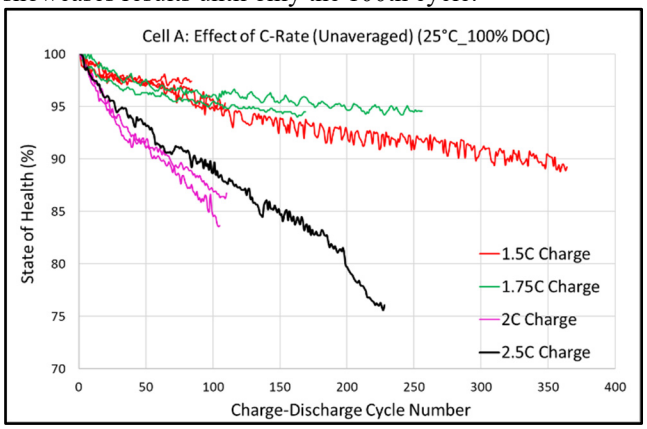

Fig. 8. Effect of charge rate on the SOH degradation for cell A

The trends seen depict that the samples tested with 1.5C and 1.75C charge rate have the same rate of degradation, which is much lower than that of the samples tested at 2C and 2.5C, which have a similar and much steeper slope of the degradation profile. Thus, SOH degradation does not increase proportionally to the increase in C-rate, but rather increases in a step manner, wherein the samples tested at 2C and 2.5C have similar rates of degradation, which is much higher than that of 1.5C and 1.75C.

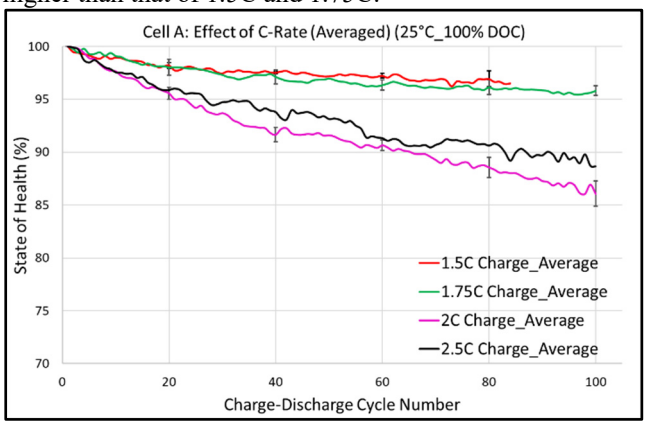

Fig. 9. Effect of charge rate on the SOH degradation for cell A (avg data)

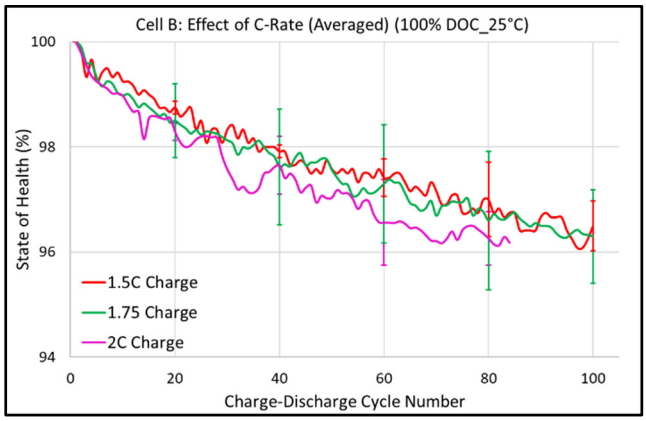

Fig. 10. Effect of charge rate on the SOH degradation for cell B (avg data)

Fig. 10 shows the effect of C-rate on the degradation profile for cell B. Three C-rates have been tested for cell B, namely 1.5C, 1.75C and 2C. The curves included in Fig. 10 are averages of the degradation plots for multiple samples tested for each C-rate along with their standard deviation error bars. As can be seen, for cell B, the C-rate does not have too significant effect on the rate of SOH degradation as the curves for all three cases have a similar slope throughout the accelerated life cycling duration.

D. SOH Degradation: Effect of Dynamic Charging

Tests with the dynamic charging profile described earlier were conducted at ambient temperature for cell A with a 2C C-rate (180 mA) as the initial charge current. After the capacity of the cell being tested below 80 mAh, the 2C charge current was accordingly changed to 160 mA. Three samples were tested for the dynamic charge profile up to over 300 cycles and their degradation plots are presented in Fig. 11 along with constant 2C and 1.75C C-rate cases for comparison. Fig. 12 plots the average of the multiple curves for individual test cases for clearer comparison. In both Fig. 11 and Fig. 12, the drop line for the 2C dynamic charge profile curves indicates the cycle number at which the battery capacity dropped below 80 mAh and the charge current changed from 180 mA to 160 mA. It can be observed that, prior to C-rate transition, the rate of degradation of the 2C

dynamic charge profile curve was similar to that of the constant 2C C-rate curve whereas after the transition it changed to the slope of the constant 1.75C C-rate degradation profile. This distinction is made more prominent in Fig. 13 which plots the average SOH drop per charge-discharge cycle for all the three cases before and after the current transition of the 2C dynamic charge profile.

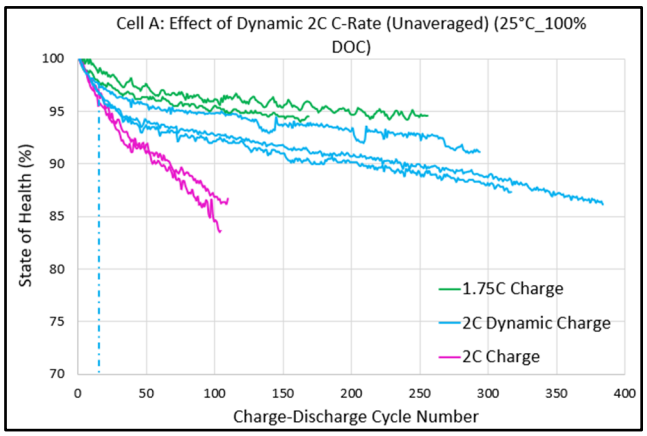

Fig. 11. Effect of dynamic 2C C-Rate on the SOH degradation for cell A

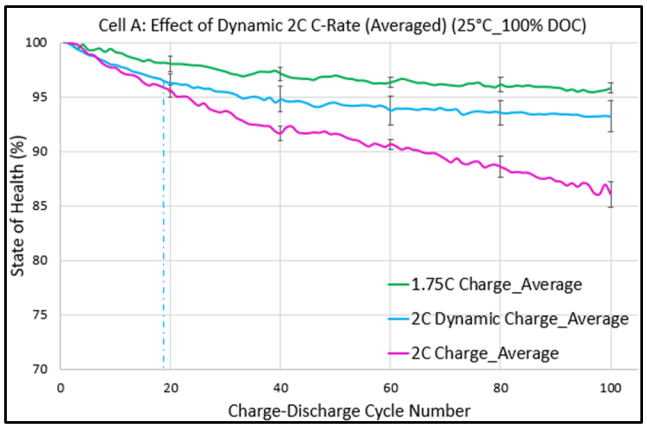

Fig. 12. Effect of dynamic 2C C-Rate on the SOH degradation for cell A (averaged data)

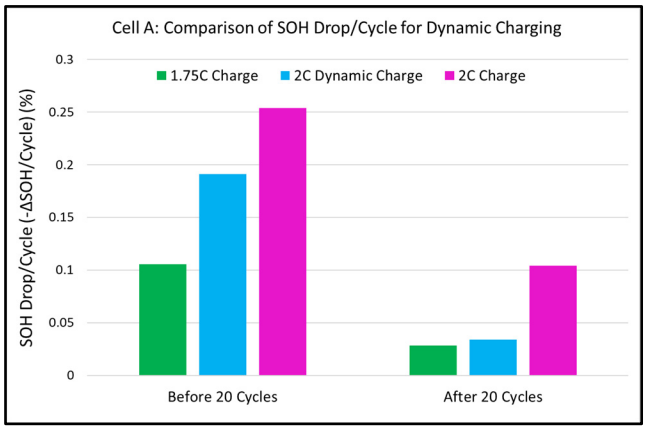

Fig. 13. Comparison of SOH drop/cycle for constant dynamic C-rate

E. SOH Degradation: Effect of Depth of Charge

Fig. 14 shows the effect of varying depth of charge for cell A. This investigation has been performed for three depths of charge, namely 50%, 75% and 100%, or deep cycling. A clear trend can be observed in the chart that deep cycles have a much drastic effect on battery SOH degradation as compared to that of cycles with low depth of charge (shallow charge cycles).

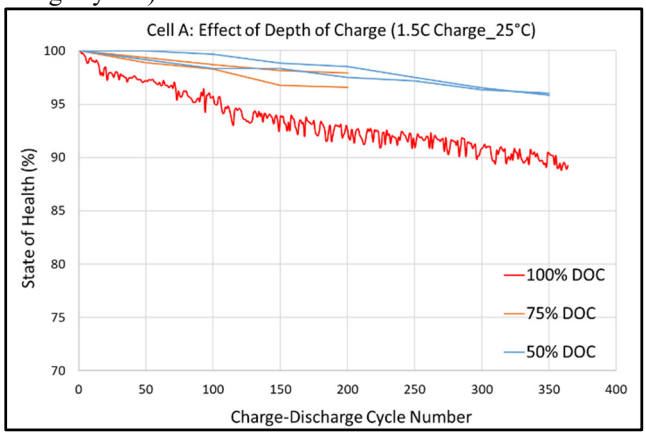

Fig. 14. Effect of depth of charge on the SOH degradation for cell A

F. Effect of Operating Temperature on SoH (Cell A)

Fig. 15 shows the effect of operating temperature on cell A's degradation profile for samples deep cycled at 298 K (ambient environment) and 313 K with 1.5C C-rate. Initially, the rate of degradation of the sample tested at 313 K is higher than that of that tested at ambient temperature. However, as the accelerated life cycling progresses, the degradation rate of the sample tested at 313 K reduces to become similar to the ambient environment sample.

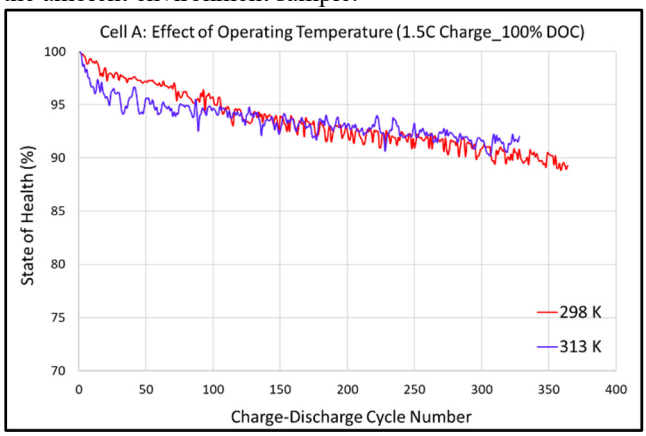

Fig. 15. Effect of operating temperature on the SOH degradation for cell A

G. SOH Degradation: Combined Effect of Operating Temperature and Dynamic Charging Profile (Cell B)

Fig. 16 shows the effect of elevated operating temperature and its combination with dynamic 2C charge on cell B. The magenta curve in the chart represents the SOH degradation profile at 25 °C and is included for the purpose of comparison. In all the plots at elevated temperatures, a steep drop in SOH after 200 charge discharge cycling is observed. In the cases with combined dynamic 2C C-rate and elevated operating temperature, the drop is delayed by a few cycles, but the nature of the steep drop is the same.

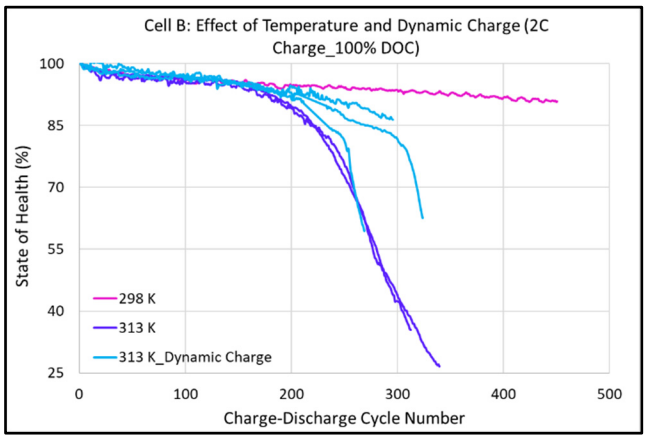

Fig. 16. Effect of operating temperature and dynamic 2C C-rate on the SOH degradation for cell B

IV. Discussion

The current section focuses on the electrochemistry underlying the degradation trends which are observed during the experimentation phase for both cell A and cell B. It is widely accepted in lithium-ion battery degradation literature that the primary cause of the battery capacity fade during long term cycling is the formation of Solid Electrolyte Interphase (SEI) film on the anode-electrolyte interface [15]. The SEI layer is formed as a result of the chemical interaction between the electrolyte and the anode surface and its formation leads to the decomposition of the electrolyte as well as the consumption of cyclable Li^+ ions. The electrochemistry of SEI formation explains most of the degradation behaviors which are observed in the current work and will be discussed in the current section.

Kolzenberg [16] studied the SEI formation in Li-ion batteries and proposed a physics-based model for the same, which explains the effect of discharge and charge rate on SEI formation and ultimately SOH degradation. They showed that the rate of SEI formation is directly proportional to the concentration of neutral Li atoms at the anode-electrolyte interface (see (13)).

$$j_{SEI} = \frac{c_{Li} D F^2 j_{int}}{2RT\kappa_{Li^+,SEI}} e^{-\eta_{SEI}} \quad (13)$$

In (13) j_{SEI} represents the rate of SEI formation, c_{Li} represents the concentration of lithium atoms at the anode-electrolyte interface, j_{int} is the intercalation rate of Li-ions in the anode which is equivalent to the charge C-rate, η_{SEI} is the overpotential for the SEI layer formation, $\kappa_{Li+,\ SEI}$ is the conductivity of the Li-ions in the SEI layer, T is the absolute operating temperature, and D, F, and R are the diffusion coefficient, Faraday constant and the universal gas constant, respectively. Now, as per the working of Li-ion batteries, during discharging, the Li-ions migrate towards the cathode due to which the Li atom concentration at the anode-electrolyte interface reduces, which in turn reduces the rate of formation of SEI layer. Hence, discharge C-rate does not contribute to SEI layer growth and hence does not affect the SOH degradation of the Li-ion battery.

On the contrary, during charging of Li-ion battery, the Li^+ ions migrate toward the anode, and intercalate with the electrons in the anode to form Li atoms, thereby increasing the concentration of Li atoms at the anode-electrolyte interface and ultimately provide impetus to the SEI layer growth. Furthermore, as the rate of SEI formation is proportional to the rate of Li-ion intercalation in the anode i.e., the charge C-rate, higher currents lead to faster formation of thick SEI layers which accelerate the SOH drop of the battery. Thus, this explains the effect of charge and discharge C-rate on SOH drop seen in cell A and cell B.

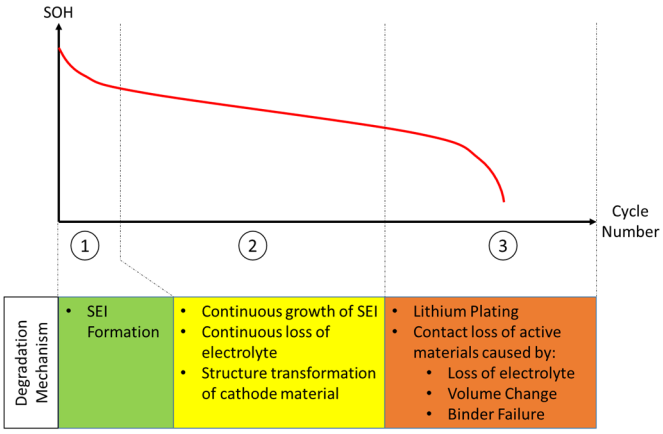

Fig. 17. The stages of SEI growth and capacity degradation throughout the life cycling of Li-ion battery [17]

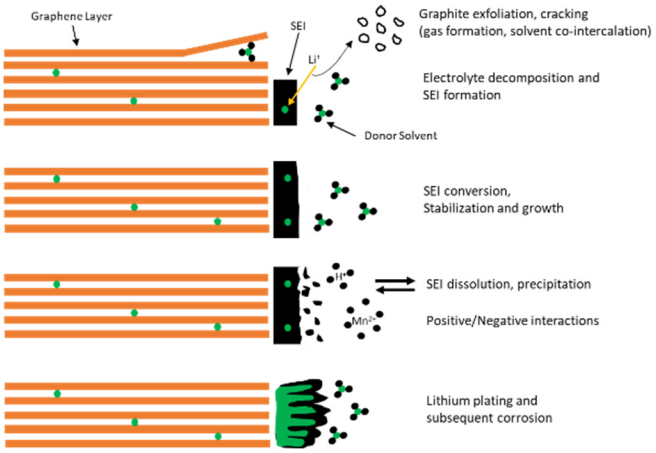

Fig. 18. Schematic of SEI initialization, growth, and subsequent Li-plating [18]

From the Fig. 14 which depicts the effect of depth of charge on cell A, the SOH drop due to initial cycling is lower for low depth of charge cases as compared to the drop for the high depth of charge case. Also, during further long-term cycling, the rate of degradation is slightly higher for the high depth of charge cases than the low depth of charge case. This behavior can also be explained using (13). A low depth of charge indicates that during charging, only limited amount of Li^+ ions are transferred to the anode, resulting in a low amount of Li atom concentration at the anode-electrolyte interface and thus a low rate of SEI formation, and vice versa for a high depth of charge scenario.

As seen in the literature, elevated temperatures generally accelerate SEI formation [15]. (13) depicts an inverse relation of SEI formation rate with absolute temperature, but an increase in the temperature would also alter other

parameters in the equation resulting in a trade-off situation. As seen for cell A in Fig. 15, an elevated temperature of 40℃ causes an initial increased rate of degradation for a few cycles which then stabilizes as the cycles progress. More samples would be tested of cell A to confirm the behavior of the degradation profile under elevated temperature.

For cell B, an elevated temperature of 40℃ seems to have no effect for the first couple of hundred cycles but following that, a steep drop in SOH is observed for all the cases tested. This can be attributed the emergence of lithium plating after prolonged cycling of graphite/NMC based Li-ion batteries [19]. Lithium plating occurs after prolonged cycling even at moderate temperatures and charging currents due to severe deterioration of ionic kinetics and graphite active material loss. This can also lead to a positive feedback loop for SEI growth if the plated lithium loses its conductive connection with graphite. Fig. 17 and Fig. 18 demonstrate the nature of degradation curve due to long term cycling and the stages of SEI formation respectively.

Thus, the degradation profile for cell B seen at elevated temperatures correlates with the nonlinear capacity fade behavior observed for Li-ion batteries due to lithium plating induced by prolonged cycling.

V. SOH Degradation Modelling

A. Use Parameter based Regression Model for SOH

The state of health model equation and the generated experimental data for cell A were subjected to a nonlinear regression run on MATLAB. A total of 4105 datapoints from 16 test samples were used for model building. Following is the model equation with the generated coefficients (14):

$$SOH = 100 - 3.75N^{0.47}C^{2.17}e^{-3932(\frac{1}{298}-\frac{1}{T})}IV^{6.1} \quad (14)$$

TABLE VI depicts the standard p-Values of the generated coefficients which are represented as b_i's as represented in (8).

TABLE VI. Regression Model Coefficients and Parameters for Cell A

Sr. No.	Coefficient/ Exponent	Variable	p-Value
1	b0	-	0
2	b1	N	0
3	b2	C	0
4	b3	T	0
5	b4	IV	0.098
RMS error in estimated SOH = 1.81%			
Model R-squared Value: 79.8%			

RMS error of the SOH values estimated by the model was found to be 1.81% and its R-Squared value is 79.8%. Furthermore, the data for cell A was also subjected to a 10-fold cross-validation procedure which yielded an average RMS error for all 10 runs as 1.81%. A similar SOH model is developed for cell B using 2173 datapoints from 14 test samples and the resultant equation (15) is:

$$SOH = 100 - 6.1N^{0.52}C^{0.48}IV^{1.75} \quad (15)$$

Operating temperature was not considered as a predictor variable in this model because of its irregular degradation effects on the SOH. TABLE VII depicts the standard p-Values of the generated coefficients which are represented as b_i's as represented in (8).

TABLE VII. Regression Model Coefficients and Parameters for Cell B

Sr. No.	Coefficient/ Exponent	Variable	p-Value
1	b0	-	0
2	b1	N	0
3	b2	C	0
5	b3	IV	0
RMS error in estimated SOH = 0.51%			
Model R-squared Value: 94%			

RMS error of the SOH values estimated by the model was found to be 0.51% and its R-Squared value is 94%. Furthermore, the data for cell b was also subjected to a 10-fold cross-validation procedure which yielded an average RMS error for all 10 runs as 0.51%. The equality of the cross-validation error and the full model error for both cells A and B are a testimony to their robustness.

VI. Summary and Conclusion

In this paper, the effect of charging-discharging current, operating temperature, depth of charge and discharge, and dynamic charge profile on the state of health degradation of coin format Li-Ion batteries has been investigated. Following are the key takeaways from the entire study: discharging current does not affect the SOH degradation but charging current increases it greatly; deeper depth of charge also leads to drastic degradation of battery SOH; for cell A, a higher operating temperature does not have too much of an effect on degradation, whereas for cell B, a higher operating temperature of 40℃ leads to a steep drop in SOH after long-term charge-discharge cycling presumably due to aging induced lithium plating. The collected data was then used to generate a model to predict the battery state of health given the aforementioned use parameters as inputs. A nonlinear regression run was performed on the data and the generated model correctly represented the trends seen in the gathered data. Furthermore, an SOH estimation model based only on the C-rate and charge time of the battery was devised for both the cells which could be used for implementation in battery management systems.

References

[1] X. Luo, J. Wang, M. Dooner, and J. Clarke, "Overview of current development in electrical energy storage technologies and the application potential in power system operation," Appl. Energy, vol. 137, pp. 511–536, January 2015.

[2] N. Nitta, F. Wu, J.T. Lee, and G. Yushin, "Li-ion battery materials: present and future," Mater. today, vol. 18, no. 5, pp. 252–264, June 2015.

[3] G. Zhou, F. Li, and H. Cheng, "Progress in flexible lithium batteries and future prospects," Energy Environ. Sci., vol. 7, no. 4, pp. 1307-1338, November 2014.

[4] J.D. MacKenzie, and C. Ho, “Perspectives on energy storage for flexible electronic systems,” Proc. IEEE, vol. 103, no. 4, pp. 535-553, April 2015.
[5] Y. Wang, B. Liu, Q. Li, S. Cartmell, S. Ferrara *et al.*, “Lithium and lithium ion batteries for applications in microelectronic devices: A review,” J. Power Sources, vol. 286, pp. 330–345, July 2015.
[6] T. Waldmann, M. Wilka, M. Kasper, M. Fleischhammer, and M. Wohlfahrt-Mehrens, “Temperature dependent ageing mechanisms in Lithium-ion batteries – A Post-Mortem study,” J. Power Sources, vol. 262, pp. 129–135, September 2014.
[7] L. Bodenes, R. Naturel, H. Martinez, R. Dedryvere, M. Menetrier *et al.*, “Lithium secondary batteries working at very high temperature: Capacity fade and understanding of aging mechanisms,” J. Power Sources, vol. 236, pp. 265–275, August 2013.
[8] F. Leng, C.M. Tan, and M. Pecht, “Effect of Temperature on the Aging rate of Li Ion Battery Operating above Room Temperature,” Sci Rep, vol. 5**,** article no. 12967, February 2015.
[9] A. Tomaszewska, Z. Chu, X. Feng, S. O’Kane, X. Liu *et al.*, “Lithium-ion battery fast charging: A review,” eTransportation, vol. 1, August 2019.
[10] Y. Li, K. Liu, A.M. Foley, A. Zulke, M. Berecibar *et al.*, “Data-driven health estimation and lifetime prediction of lithium-ion batteries: A review,” Renew. Sust. Energ. Rev., vol. 113, October 2019.
[11] J. Hoog, J. Timmermans, D. Stroe, M. Swierczynski, J, Jaguemont *et al.*, “Combined cycling and calendar capacity fade modeling of a Nickel-Manganese-Cobalt Oxide Cell with real-life profile validation,” Appl. Energy, vol. 200, pp. 47-61, August 2017.
[12] D. Stroe, M. Swierczynski, A. Stan, R. Teodorescu, and S.J. Andreasen, “Accelerated Lifetime Testing Methodology for Lifetime Estimation of Lithium-Ion Batteries Used in Augmented Wind Power Plants,” IEEE Trans. Ind., vol. 50, no. 6, pp. 4006-4017, April 2014.
[13] E. Sarasketa-Zabala, E. Martinez-Laserna, M. Berecibar, I. Gandiaga, L.M. Rodriguez-Martinez *et al.*, “Realistic lifetime prediction approach for Li-ion batteries,” Appl. Energy, vol. 162, pp. 839-852, January 2016.
[14] P. Lall, V. Soni, A. Abrol, B. Leever, S. Miller, “Effect of Charge-Discharge Depth and Environment Use Conditions on Flexible Power Sources,” *Proc. ASME. InterPACK,* Anaheim, CA, USA, 2019.
[15] M.M. Kabir, and D.E. Demirocak, “Degradation mechanisms in Li-ion batteries: a state-of-the-art review,” Int. J. Energy Res., vol. 41, no. 14, pp.1963– 1986, April 2017.
[16] L. von Kolzenberg, A. Latz, and B. Horstmann, “Solid-electrolyte interphase during battery cycling: theory of growth regimes,” Chem Sus Chem, vol. 13, no. 15, article no. 3901, May 2020.
[17] X. Han, L. Lu, Y. Zheng, X. Feng, Z. Li *et al.*, “A review on the key issues of the lithium ion battery degradation among the whole life cycle,” eTransportation, vol. 1, article no. 100005, August 2019.
[18] J. Vetter, P. Novak, M.R. Wagner, C. Veit, K.C. Moller *et al.*, “Ageing mechanisms in lithium-ion batteries,” J. Power Sources, vol. 147, no. 1-2, pp. 269-281, September 2005.
[19] S.F. Schuster, T. Bach, E. Fleder, J. Muller, M. Brand *et al.*, “Nonlinear aging characteristics of lithium-ion cells under different operatinal conditions,” J. Energy Storage, vol. 1, pp.44-53, June 2015.